ACS SENSORS

pubs.acs.org/acssensors

Article

Multilayer Double-Sided Microstructured Flexible Iontronic Pressure Sensor with a Record-wide Linear Working Range

Yan Xiao, Yu Duan, Ning Li, Linlin Wu, Bo Meng, Feihu Tan, Yan Lou, Hao Wang, Weiguan Zhang,* and Zhengchun Peng*

Cite This: *ACS Sens.* 2021, 6, 1785−1795

Read Online

ACCESS | Metrics & More | Article Recommendations | Supporting Information

ABSTRACT: Wearable electronics, electronic skins, and human−machine interfaces demand flexible sensors with not only high sensitivity but also a wide linear working range. The latter remains a great challenge and has become a big hurdle for some of the key advancements imperative to these fields. Here, we present a flexible capacitive pressure sensor with ultrabroad linear working range and high sensitivity. The dielectric layer of the sensor is composed of multiple layers of double-sided microstructured ionic gel films. The multilayered structure and the gaps between adjacent films with random topography and size enhance the compressibility of the sensor and distribute the stress evenly to each layer, enabling a linear working range from 0.013 to 2063 kPa. Also, the densely distributed protrusive microstructures in the electric double layer contribute to a sensitivity of 9.17 kPa^{-1} for the entire linear working range. For the first time, a highly sensitive pressure sensor that can measure loading conditions across 6 orders of magnitude is demonstrated. With the consistent and stable performance from a low- to high-measurement range, the proposed pressure sensor can be used in many applications without the need for recalibration to suit different loading scenarios.

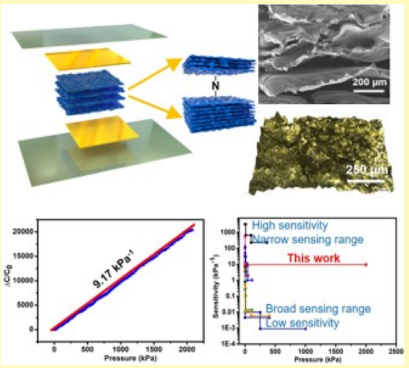

KEYWORDS: *flexible pressure sensor, ultrabroad linear working range, multilayer double-sided microstructures, iontronic sensor, high sensitivity*

Pressure sensors with flexible and stretchable characteristics have great potential for applications in human health monitoring,[1−3] electronic skin of robots,[4−7] and human−machine interfaces,[8−10] owing to their conformal attachment with various curved surfaces for accurate sensing of stimuli. The pressure from a stimulus in different applications, sometimes even in the same field, may vary greatly. For instance, in health monitoring, the respiration system often generates a pressure <1 kPa, while a pulse from 1 to 10 kPa, body motion from 10 to 500 kPa, orthopedic operations >500 kPa, and so forth.[11−14] In practical applications, a pressure sensor with poor linearity in the working range often needs to be recalibrated to suit for different loading conditions, which requires extra electrical circuits and signal-processing software.[15] Besides, the preloading during sensor packaging is often unavoidable, which further compromises the linear working range, making the application of the sensor for low-pressure level measurement even more difficult. Thus, developing a flexible pressure sensor with high sensitivity and wide sensing range that one calibration can work for different loading conditions is highly desired.

Numerous flexible pressure sensors based on different signal transduction modes, including piezoresistivity,[16−19] capacitance,[20−22] piezoelectricity,[23−25] and triboelectricity,[26,27] have been developed for the aforementioned applications. The capacitive pressure sensors have the advantages of a simple structure configuration and stable (low drift) performance, making them the most popular flexible pressure sensors among all types of pressure transducers. However, the sensitivity of a flexible piezo-capacitive sensor is often limited by the low dielectric constant of most flexible dielectric materials such as elastomers and gels.[28−30] Differing from traditional dielectric materials, ion gel incorporates an elastomer with an ionic liquid to work as the dielectrics. Because of the high interfacial capacitance of the electric double layer (EDL) at the dielectric/electrode, that is, iontronic, the interface can effectively enhance the sensitivity of the sensor.[31,32] As such, ion gel is a promising alternative dielectric material for fabricating high-performance capacitive flexible sensors.

To further enhance the performance of an iontronic capacitive sensor, one could introduce and engineer microstructures inside the EDL, which determines the capacitance change under pressure loading. For example, Cho et al.[33]

Received: December 5, 2020
Accepted: April 22, 2021
Published: May 5, 2021

https://doi.org/10.1021/acssensors.0c02547
ACS Sens. 2021, 6, 1785−1795

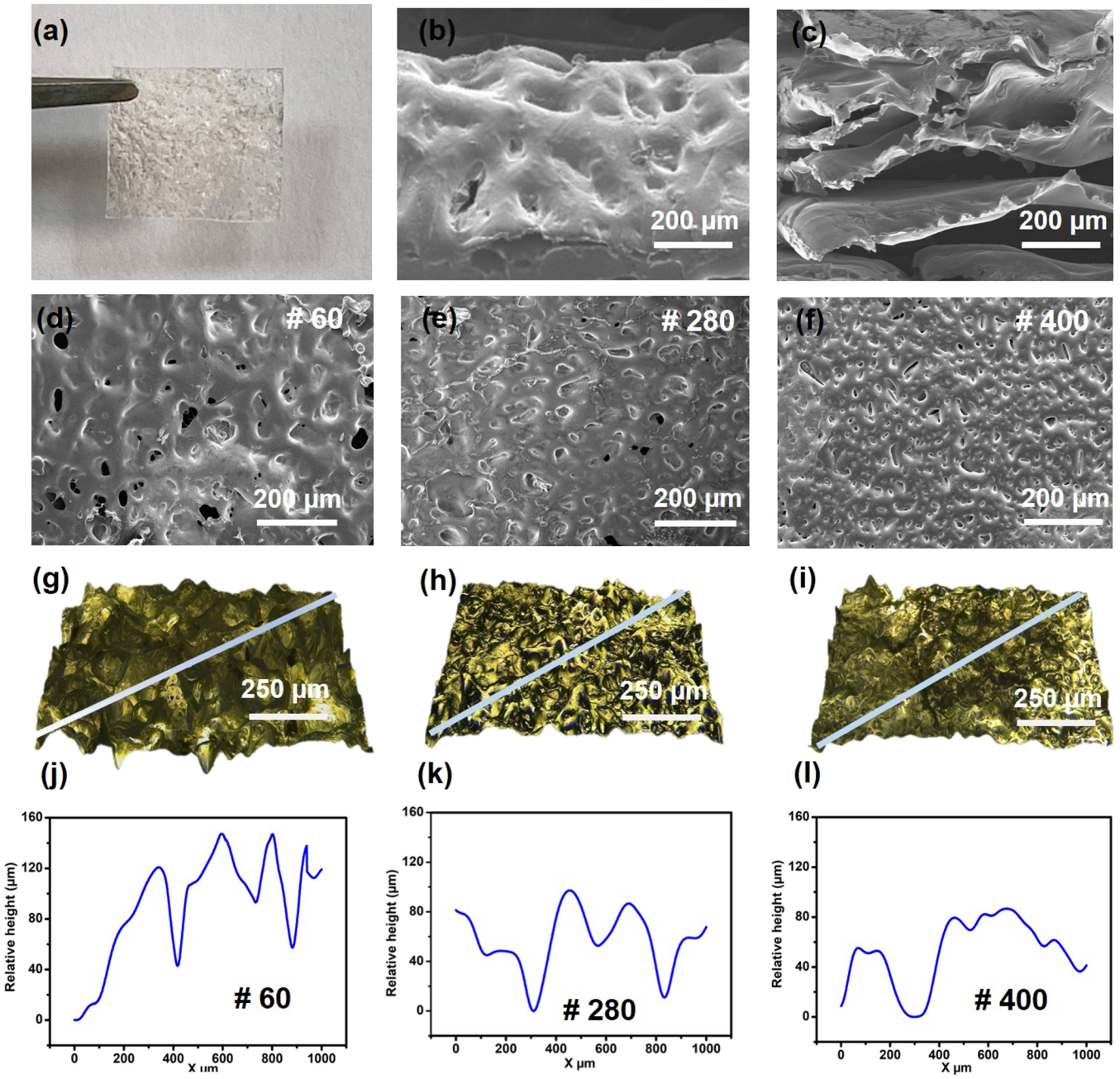

Figure 1. (a) Characterization of the prepared MDM iontronic film with 12 layers. (a) Photo image of the as-fabricated MDM iontronic film by using # 400 sandpaper as a template. (b) Titled and (c) cross-sectional SEM image of the corresponding film by using # 400 sandpaper as the template; (d–f) Top-view SEM image of the MDM iontronic film demolded from different grit number sandpaper (d) #60, (e)# 280, and (f) #400; and (g,h) 3D morphology and (j,i) their corresponding height profile across the diagonal of the top layer prepared by using different grit number sandpaper as the template: (d) and (j) #60, (h) and (k) #280, and (i) and (l) #400.

reported an iontronic sensor by patterning micropyramids on the ionic gel surface and achieved a high sensitivity of 41.64 kPa^{-1} from 0 to 0.5 kPa. Qiu et al.[34] reported a high sensitivity of 54.31 kPa^{-1} within 0.5 kPa by constructing microcones on the iontronic film surface using a calathea zebrine leaf as the template. Chhetry et al.[35] enhanced the sensitivity to 131 kPa^{-1} up to 2 kPa employing randomly distributed microstructures on an iontronic film surface. Because these microstructures are easily compressed, the sensors saturate under very light pressure loading, which limits their usefulness to a very narrow window of applications. To solve this problem, Bai et al.[36] proposed graded intrafillable microstructures on the ion gel surface to improve the compressibility of the iontronic layer. With such design, ultrahigh sensitivity (3302.9 kPa^{-1}) and a broad sensing range (0.08 pa–360 kPa) were obtained. However, the sensitivity divided into three segments declined rapidly when loading pressure exceeds 10 kPa. Li et al.[37] developed a low-cost iontronic sensor by dispersing commercial paper into ion gel solution followed by drying. A linear working range up to 25 kPa and a sensitivity of 10 nF kPa^{-1} cm^{-2} were achieved. To date, the tradeoff between the sensitivity and the linear working range is still a significant challenge for a flexible pressure sensor.

https://doi.org/10.1021/acssensors.0c02547
ACS Sens. 2021, 6, 1785–1795

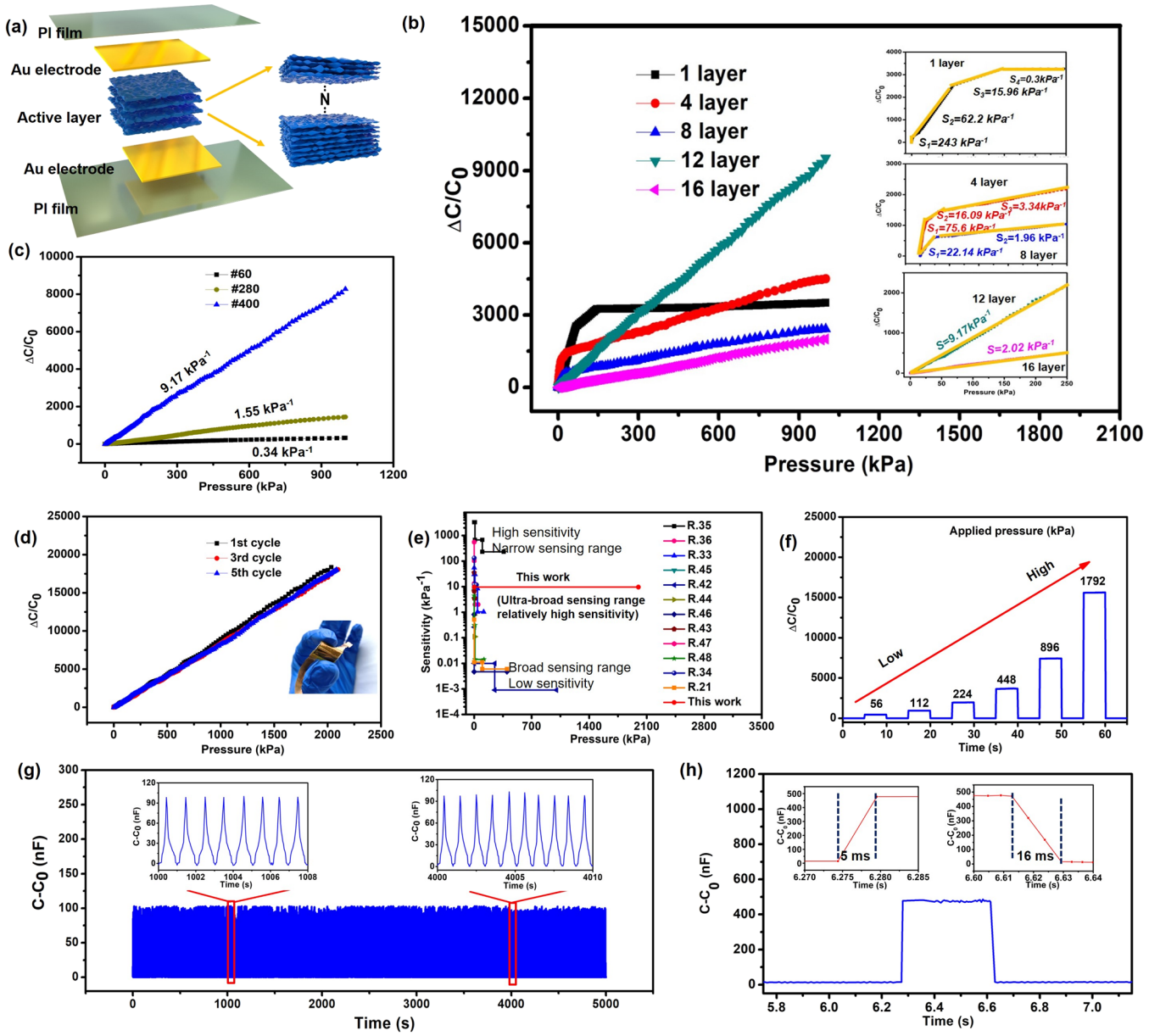

Figure 2. Characterization of the MDM iontronic pressure sensors. (a) Schematic illustration of the flexible capacitive pressure sensor based on the MDM iontronic films; (b) relative capacitance change vs pressure applied to the MDM iontronic pressure sensor using 1, 4, 8, 12, and 16 layers of iontronic films; the template is a grit #400 sandpaper. (c) Relative capacitance change vs the pressure applied to the MDM iontronic pressure sensor prepared using different sandpaper (#60, #280, and #400) as the template. All of the sensors had 12 layers of iontronic films. (d) Cyclic test of the sensor made using grit #400 and 12 layers of iontronic films, and the inset is the photograph of the corresponding sensor. (e) Comparison of the sensor sensitivity and linear region between our work and other studies. (f) Relative capacitance change with stepwise increasing pressure. (g) Stability test over 5,000 cycles under a pressure of 60 kPa. (h) Response time of the sensor.

Multilayer design can buffer the applied pressure to a larger extent than its single-layer counterpart. Therefore, such a strategy is often employed by researchers to improve the linear working range of flexible pressure sensors. For example, Lee et al.[38] designed a multilayer microdome structure to broaden the linear working range from 0 to 353 kPa, with a high sensitivity of 47.7 kPa^{-1} in the entire working range. Based on this principle, Pyo et al.[39] reported an ultrawide linear range (0.2−982 kPa) with a sensitivity of 26.13 kPa^{-1} by using multilayered fabric as the active layer. However, the transduction mode of the above-mentioned sensors relies on a piezo-resistive mechanism with drawbacks of high drift and hysteresis.[40,41] Besides, the above sensors are still not capable of measuring pressure that exceeds 1000 kPa, which is common in scenarios such as cardiopulmonary resuscitation (CPR) operation, and boxing punches, as well as tactile operation of industrial robots.

In this study, we propose a flexible capacitive pressure sensor with multilayer double-sided microstructured (MDM) iontronic films as the dielectric layer. The multilayered design and random form of protrusive microstructures between the adjacent iontronic films play a crucial role in distributing the pressure loading and enhancing the structural compressibility, resulting in an ultrabroad linear working range exceeding 2000 kPa. Also, the densely distributed protrusive microstructures within the EDL at the interface contribute to high sensitivity

https://doi.org/10.1021/acssensors.0c02547
ACS Sens. 2021, 6, 1785−1795

($\sim$10 kPa^{-1}) within the entire linear working range. The sensor also demonstrates a fast response time and excellent mechanical stability. Hence, the proposed sensor has great potential in providing a more capable interface for human–machine interaction, expanding the tactile function of both industrial and service robots, as well as other applications.

EXPERIMENTAL SECTION

Preparation of the Ion Gel. The ion gel used for the iontronic film fabrication was prepared using a polymerization method as reported by Chhetry et al.[35] A poly(vinylidene fluoride-*co*-hexafluoropropylene) (Sigma-Aldrich) P(VDF-HFP)-based ion gel was employed in this study. The ionic gel film is composed of a structuring polymer and an ionic liquid (IL). Figure S1a shows the molecular structures of [P(VDF-HFP)] and 1-ethyl-3-methylimidazolium bis(trifluoromethylsulfonyl)imide ([EMIM][TFSI]) that are mixed to form the ion gel. Specifically, a 15% weight ratio of P(VDF-HFP) was added to acetone and stirred at 25 °C for 4 h until it dissolved. Then, [EMIM][TFSI] with a 45% weight ratio was added to the as-prepared P(VDF-HFP) solution to form a polymer/ILs mixture by stirring for 30 min.

Fabrication of the MDM Iontronic Dielectric Layer. The iontronic film with double-sided microstructures was prepared by demolding twice from the sandpaper under controlled semicuring to the curing status of the polymer/ILs mixture. Afterward, the entire dielectric layer was fabricated by stacking multiple layers of the double-sided microstructured iontronic films with a repeated process. Figure S1b displays the detailed fabrication process of the MDM iontronic dielectric layer and its sensor. The sandpaper was cut into a 10 mm × 10 mm piece and treated with an antiadhesion agent (trichloro(1*H*,1*H*,2*H*,2*H*-perfluorooctyl)silane) for easy peel-off. Subsequently, a volume of 0.5 mL polymer/ILs mixture was dip-coated on the prepared sandpaper and spun at 500 rpm for 30 s. Then, another piece of sandpaper was covered on a top surface of the ion gel and heated at 80 °C for 10 s together to duplicate the microstructure on semicured ion gels. Peeling off the sandpaper on the top surface, and the fabrication of the first double-sided microstructured iontronic layer were accomplished. Instantly, the second layer was prepared by directly covering the first layer, which formed a face-to-face configuration of microstructures on each side. Then, the stacked sample was heated at 80 °C for 5 min to stick the first and second layers firmly. The MDM iontronic dielectric layers were fabricated by repeatedly stacking them layer-by-layer as mentioned above. Finally, the as-prepared sample was heated at 80 °C for 24 h to fully remove the rest of the solvent and then the sandpaper under the first layer was removed. Based on this fabrication method, a total thickness of a 12-layered iontronic film is about 1 mm that each layer is firmly stacked together. No debonding was found during utilization. The surface roughness is determined by the dimensions of the protrusion-like structures from the sandpaper. We engineered different roughness by using sandpapers with different mesh numbers of sandpaper, #60, #280, and #400 as a template, wherein the larger number represents lower roughness.

Characterization and Measurement of the MDM Iontronic Pressure Sensor. The structure morphology and surface roughness of the iontronic dielectric layer were characterized using an optical microscope (Leica DM6B), integrated with a 3D imaging analysis system, and a field-emission scanning electron microscope (FE-SEM, Hitachi SU8010). The MDM iontronic pressure sensor was packaged by following the parallel-plate capacitor configuration. The flexible electrodes were prepared by thermally evaporating 200/10 nm thick Au/Cr on a 25 μm thick polyimide (PI) film and cut into 10 mm × 10 mm pieces. Afterward, the pressure sensor was mounted on a flat stage of the dynamic and fatigue testing system (ElectroPuls 1000, Instron) for sensitivity characterization. Controllable dynamic and static press loading can be applied to the sensor through a customized acrylic cubic probe (1 cm^2 in area) clamped on the upper gripper of the instrument. Moreover, the real-time capacitance variation was measured using a precision impedance analyzer (6500B, Wayne Kerr). The response time and application tests were measured using a digital multimeter (DMM6500, Keithley).

RESULTS AND DISCUSSION

Figure 1a shows the photo image of the as-prepared MDM iontronic film demolded from #400 sandpaper. The film still demonstrates good transparency after the stacking of multiple microstructured layers. The tilt-view SEM image of Figure 1b shows the surface topography of the MDM iontronic film fabricated by using #400 sandpaper as a template. Graded protrusions with several tens of micrometers located randomly on the film surface. The cross-sectional view of the MDM iontronic film in Figure 1c exhibits a clear boundary between the adjacent stacking films. Gaps between two adjacent films were formed and have different dimensions, because of the random distribution of protrusive microstructures. Figure 1d–f compares the SEM images of the iontronic dielectric layer demolded from the #60, #280, and #400 sandpaper, respectively. The density of the microstructures increased as the grit number of the sandpaper increased from 60 to 280 and 400, meanwhile, the dimension of these protrusive microstructures decreased. The surface roughness of the iontronic dielectric layer, demolded from different grit sandpapers (#60, #280, and #400), was characterized using a three-dimensional (3D) image analysis system of the optical microscope. Figures 1g–i shows the 3D topography of the film demolded from #60, #280, and #400 sandpaper, and the corresponding relative heights of these protrusive microstructures are plotted in Figure 1j–l. Generally, the height profile decreases as the sandpaper grit number increases. Specifically, a profile of the iontronic dielectric layer demolded from #400 sandpaper is within the range of 0–80 μm, which is lower than those that are demolded from #60 (0–150 μm) and #280 (−0–100 μm) sandpaper.

Figure 2a shows the schematic structure of the proposed MDM iontronic capacitive pressure sensor. The number of stacked iontronic films and the size of the protrusive microstructures are systematically studied. The stacked-layer numbers of the iontronic film were first studied by fixing the surface roughness using #400 sandpaper as the template. Figure 2b shows the relative capacitance change as a function of the applied pressure from 0 to 1000 kPa, which is achieved using a different number of layers for the iontronic film as the dielectric layer. Therefore, the sensitivity of the capacitive pressure sensor can be defined as $S = (\Delta C/C_0)/\Delta P$, where ΔC is the capacitance change, C_0 is the initial capacitance without loading, and ΔP is the change of the applied pressure. From the enlarged response curves inserted in Figure 2b, four segments existed for the sensor with one-layer iontronic film. The highest sensitivity reaches to 243 kPa^{-1} within the 0–1.5 kPa range and decreased to 62.2 kPa^{-1} (1.5–16.7 kPa), 15.96 kPa^{-1} (16.7–150 kPa), and 0.3 kPa^{-1} (150–1000 kPa) with increased pressure. By stacking four layers of the iontronic film, the sensitivity divides into three parts, which decreased from 75.6 kPa^{-1} (<9.47 kPa) to 16.09 kPa^{-1} (9.47–31.4 kPa) and 3.34 kPa^{-1} (31.4–1000 kPa). The sensitivity response curve contains two parts with eight layers of iontronic films, which decreased from 22.14 kPa^{-1} (<30 kPa) to 1.96 kPa^{-1} (30–1000 kPa). When the layer number of iontronic film is 12, the relative change of the capacitance demonstrates a linear response with the increased pressure. Further increasing the layer number to 16 still allows the linear response in the entire

https://doi.org/10.1021/acssensors.0c02547
ACS Sens. 2021, 6, 1785–1795

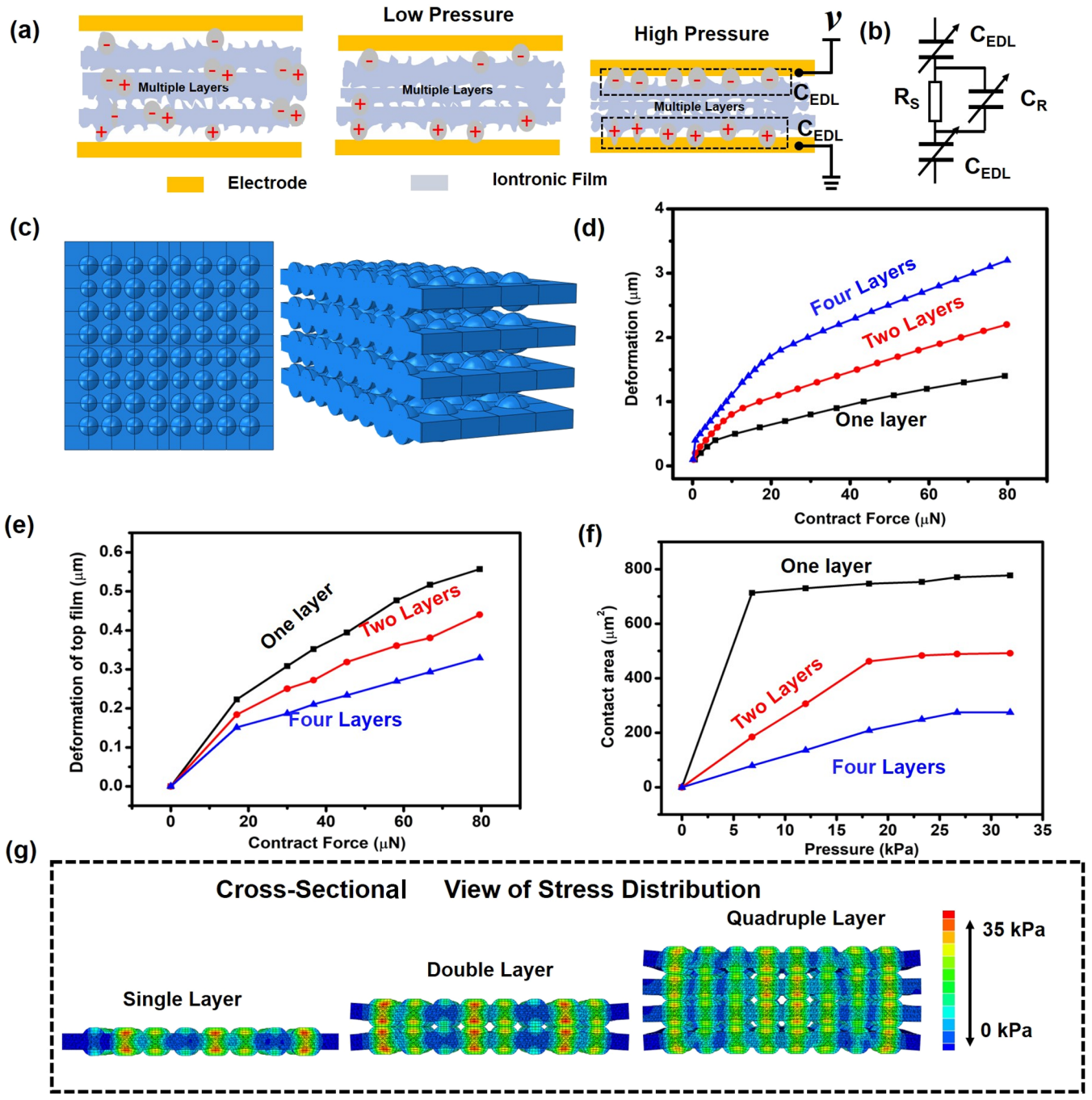

Figure 3. Sensing mechanism of the MDM iontronic pressure sensor. (a) Schematic of the charge distribution and contact area at the initial zero pressure state, low-pressure loading state, and high-pressure loading state. (b) Equivalent circuit model of MDM iontronic pressure sensor. (c) Schematic of the simulation model with random distributed microstructures. (d) Finite element calculations of the deformation of iontronic dielectric layer as a function of contact force. (e) Finite element calculations of the deformation of the top iontronic layers as a function of contact force. (f) Finite element calculations of the change of contact area as a function of contract force. (g) FEA of the stress distribution under 35 kPa external pressure with different numbers of iontronic layers as the sensor structure.

pressure range, but the sensitivity decreased from 9.17 to 2.02 kPa^{-1}.

The maximum sensitivity and its corresponding linear range of the iontronic pressure sensors with different number of layers are plotted in Figure S2. It indicates that maximum sensitivity decreases with increasing layer numbers, while the linear range increases. From eight layers to 12 layers, the linear range for maximum sensitivity expands significantly (from 30 kPa to more than 1000 kPa). We would like to point out, within the experimental interval between 8 and 12 layers, there might be another layer number already achieving more than 1000 kPa linear range with its maximum sensitivity, which would be higher than that of the 12 layered sensor (9.17 kPa^{-1}).

Previous reports[33,34] indicate that the sensitivity of the iontronic pressure sensor is determined by the change of the contact area of the EDL at the interface. To maximize such a change, we engineer the roughness of the MDM iontronic

https://doi.org/10.1021/acssensors.0c02547
ACS Sens. 2021, 6, 1785−1795

films by templating them from sandpapers of different roughness (#60, #280, and #400). A comparative study is present in Figure 2c in which the stacking number of the iontronic films is fixed at 12. From 0.013 to 1000 kPa, all the sensors exhibit excellent linearity. However, the sensitivity of the sensors varies, increasing with the smaller roughness of the iontronic films. As characterized in Figure 1j–l, sandpaper with a larger grit is made by smaller sand grains (i.e., lower height). Thus, the protrusive microstructures are denser with smaller roughness of the sandpaper, so more contact area is built at the EDL interface, leading to a larger chance of contact area under compression. Although in theory smaller roughness of the iontronic film leads to higher sensitivity, in real practice fabricating extremely small roughness by replicating microstructures from sandpaper is challenging. The smallest roughness of the iontronic film of our sensors is determined by the commercially available #400 sandpaper. As such, the sensor with the smallest roughness of the iontronic films, demolded from the #400 sandpaper, has the highest sensitivity of 9.17 kPa^{-1}.

The optimized design parameters (12 layers of iontronic films demolded from the #400 sandpaper) were selected from the above studies, and used to study the maximum linear working range of the sensor. The sensor with a square dimension of 10 mm × 10 mm was fabricated, which shows good flexibility as displayed in Figure 2d (inset). The response curves almost overlapped with each other for five cycles of loading and unloading testing up to 2000 kPa, while the sensitivity maintained at 9.17 kPa^{-1} (Figure 2d). To further investigate the linear sensing range, the applied pressure is extended to 3000 kPa, and the result in Figure S3 shows that the linear response is extended up to 2063 kPa, beyond which the sensor started to saturate with a sensitivity drop to 2.22 kPa^{-1}. The lower working limit of the sensor is determined by experiment. We started the external stimulation from 0 Pa, and gradually increased it to a higher value. From 0 to 50 Pa, the response of the sensor was measured five times and plotted in Figure S4. Noticed from this figure that the capacitance changed randomly from 0 to 13 Pa, and from 13 Pa on, the capacitance change became detectable. Hence, we determine the lower working limit of the sensor is 13 Pa. Figure 2e compares the performance of the previously reported capacitive pressure sensors with different sensitivity and linear working range. An ultrawide working range of 400 kPa has been achieved by Sharma et al.[21] and 1000 kPa by Chen et al.,[42] but the sensitivity did not exceed 1 kPa^{-1} at a low-pressure level and dropped quickly to about 10^{-3} kPa^{-1} at a high-pressure level. With sensitivity greater than 10 kPa^{-1}, the best of those studies showed a working range up to 360 kPa,[21,33−36,42−48] while our MDM iontronic capacitive pressure sensor achieved a sensitively linear working range from 0.013 to 2063 kPa. To the best of our knowledge, this has been the widest linear working range up to date. For the first time, we demonstrated a pressure sensor that can measure loading conditions across 6 orders of magnitude with a sensitivity of ∼10 kPa^{-1}.

Next, we studied the stability of the proposed sensor. As shown in Figure S5, the capacitance of the sensor overlaid with the initial value of the sensor after each cyclic test, which means the stacked MDM iontronic film can recover to its initial state after pressure is released, implying great stability of the sensor. As displayed in Figure 2f, the dynamic performance of our sensor was measured continuously under a gradually increased pressure loading. Under a step-by-step increase in pressure from 56 to 1792 kPa, the sensor exhibits a stable response to the changed loading/unloading pressure. The frequency response of the sensor applied at 1, 0.5, and 0.25 Hz under 60 kPa is demonstrated in Figure S6. The result demonstrates an accurate and stable response of the sensor at all those frequencies. A repetitive loading/unloading test was performed at a frequency of 1 Hz to evaluate the long-term stability of the sensor. Figure 2g shows the dynamic capacitance change of the sensor under 5,000 repeated loading/unloading cycles. The capacitance change at the beginning and the end of the process are shown as insets in Figure 2g, which proves the high stability of the sensor for long-term usage. Figure 2h shows the response and recovery time measured under an external pressure of 400 kPa that was calculated to be 5 and 16 ms, respectively, based on the loading and unloading processes. The ultrafast response time of the sensor is due to the rapid contact area modification of the EDL under pressure. Hysteresis of the sensor under different loading conditions is also characterized as shown in Figure S7. At high pressure loadings such as from 850 to 1000 kPa, the sensor exhibits a hysteresis of ∼16%. With low pressure loadings, the hysteresis drops quickly with much smaller lag in response.

The high sensitivity and broad linear working range of the fabricated sensor are mainly attributed to the design and optimization of the multilayer double-sided microstructures and the high dielectric constant of the iontronic films. Different from traditional dielectric films, the iontronic film introduces two distinctive EDLs at the two interfaces with electrodes,[49] which significantly increases the capacitance of the sensor when it is under compression. As shown in Figure 3a, at the initial state only a few protrusive microstructures are in contact with the electrode, and the capacitance of the sensor is low. With external pressure loading, the protrusive microstructures start to be compressed and the contact area increases, leading to an increased capacitance. In addition, the entire iontronic dielectric layer becomes thinner, which further increases the capacitance of the sensor. As a result, the change of total capacitance is magnified. Figure 3b shows the equivalent circuit model of the sensor. The device is composed of two EDL capacitors (C_{EDL}) at the interface of the top and bottom electrodes with a bulk resistance (R_s) connected in series. The overall dielectric layer is represented as a parallel-plate capacitor (C_R) in parallel with R_s. According to the Gouy–Chapman–Stern model, the areal capacitance of EDL can be roughly estimated as.[50,51]

$$C = \varepsilon/\lambda \tag{1}$$

$$\lambda = \sqrt{\frac{\varepsilon k_B T}{e^2 \sum_i z_i^2 n_i}} \tag{2}$$

where ε, λ, k_B, T, e, z_i, and n_i are the permittivity, Debye length, Boltzmann constant, temperature, the magnitude of the electronic charge, charge number of species i, and the number density of species i, respectively. The contact area between the protrusive microstructures and electrode essentially determines the EDL capacitance.[52] Here, the contact area can be approximately estimated from the surface roughness of the iontronic film. The detailed parameter values of eqs 1 and 2 are listed in Table S1 as Supporting Information. From the measured roughness in Figure 1i, the EDL capacitance of the sensor prepared with #400 sandpaper is calculated to be about

https://doi.org/10.1021/acssensors.0c02547
ACS Sens. 2021, 6, 1785−1795

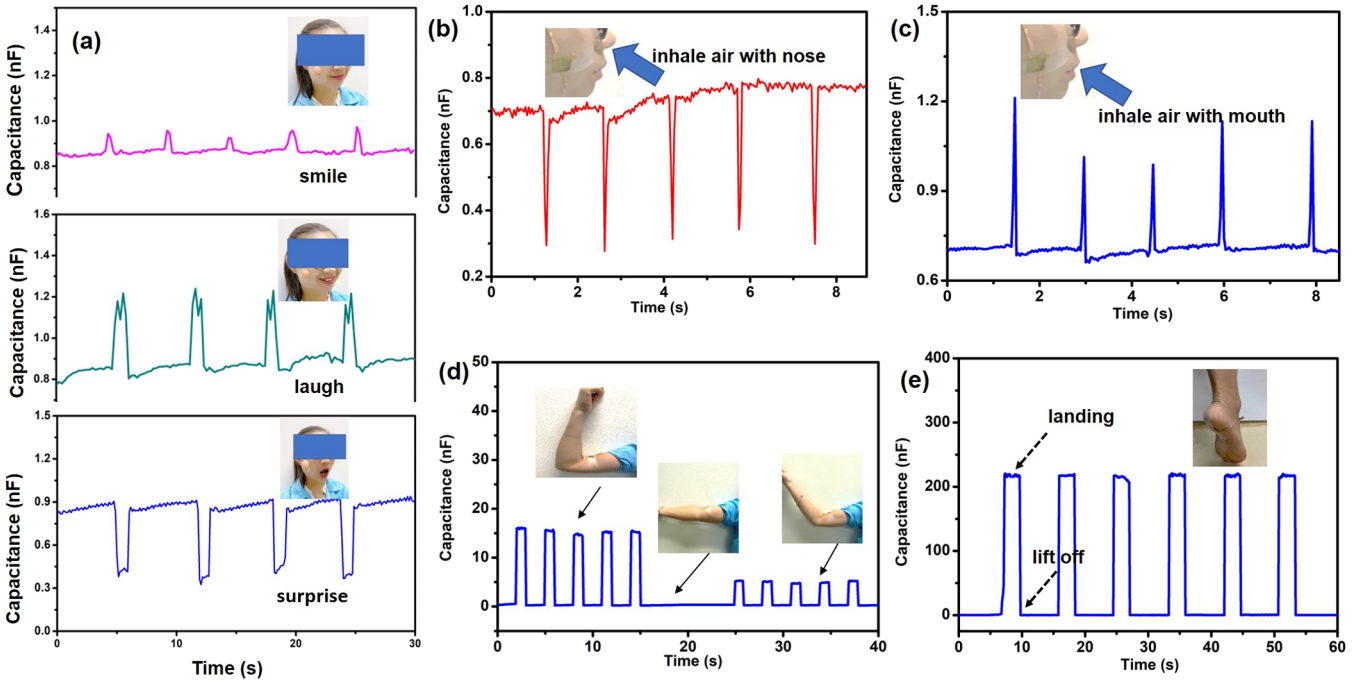

Figure 4. Detection of skin motions by the MDM iontronic pressure sensor. (a) Capacitance changes with different facial expressions. (b,c) Capacitance signal as one inhales air by nose and by mouth, respectively. (d) Capacitance changes in the elbow bending motions with different bending angles. (e) Capacitance changes in the foot motion.

200 pf. This value is consistent with the experimental data given in Figure S6. In comparison, the value of C_R can be ignored and the two EDL capacitors dominate the total capacitance of the sensor. With densely distributed protrusive microstructures inside EDL, a slight increase of pressure loading can compress a great number of microstructures, leading to a dramatic change of contact area with the electrodes. This results in a large capacitance change corresponding to high sensitivity of the sensor.

Finite element analysis (FEA) was performed on a representative model. Three different numbers (one, two, and four layers) of iontronic films with the random forms of microprotrusions on both sides of each film were studied. To save the computational resources and time cost, the simulation model was simplified as randomly distributed hemispheres sized from 1.6 to 2 μm on a 50 μm × 50 μm square film, as shown in Figure 3c. We also restricted the pressure loading up to 35 kPa in the simulation, which covers the linear range of the 8-layered sensor (corresponding to its maximum sensitivity) in the experimental results. The ionic gel was modeled as the Mooney−Rivlin material where parameters are referenced from He et al.[53] Figure 3d shows the relationship between the contact force and the deformation of the dielectric layer. The effective spring constant of the iontronic dielectric layer decreases as the number of iontronic films increases. Although the four-layer structure has larger deformation as an entity, the deformation of the top and bottom layers that contact with electrodes is smaller than that of the two-layer and one-layer structures (Figure 3e). Through Figure 3e, we found that the contact area between the microstructured iontronic film and the electrodes decreases with the increasing number of layers. Furthermore, the change of contact area between the intronic film and the electrodes determines the sensitivity of the sensor. Thus, the contact area changing under different loading conditions is extracted and plotted in Figure 3f. For reasonable computation cost, the initial contact area in the simulation was set as 0 such that the electrodes barely touch the microstructures on the very top and bottom surface of the iontronic film(s). Noted from Figure 3f, with the same contact force, the one-layered dielectric structure has the largest change of contact area with the electrode, but the smallest linear working range (0−6 kPa). The contact area becomes smaller when the layer number increases, the four-layered structure has the smallest change of the contact area while the linear range expands to 25 kPa. With this simulation, we believe the maximum sensitivity and linear range with further increase of the layer numbers will continue this trend, which may be applied to explain our experimental results shown in Figure 2b. Hence, the maximum sensitivity of multilayered iontronic pressure sensors drops with increasing number of layers.

On the other hand, the linear working range increases with the increasing number of iontronic films. Not only the lower effective spring constant allows for larger deformation of the dielectrics under the same pressure, the gaps between the adjacent iontronic films with random topography and size also help distribute the stress more uniformly, as shown by the FEA simulation in Figure 3g. As pressure is applied to the sensor, the larger protrusive microstructures that are initially in contact are deformed first, sustaining the initial pressure loading. As the pressure increases, smaller protrusive microstructures start to make contact to sustain the additional pressure. With the MDM design, the probability of creating more variation of gap topography and gap size increases remarkably. Collectively, the randomly formed gaps can support pressure loadings to a much larger extent. The benefit of multilayer double-sided microstructures includes the following: (i) more layers lead to more decrease of the effective spring constant of the entire dielectric film, allowing more compression of the device under the same loading; (ii) with more layers, the protrusive

https://doi.org/10.1021/acssensors.0c02547
ACS Sens. 2021, 6, 1785−1795

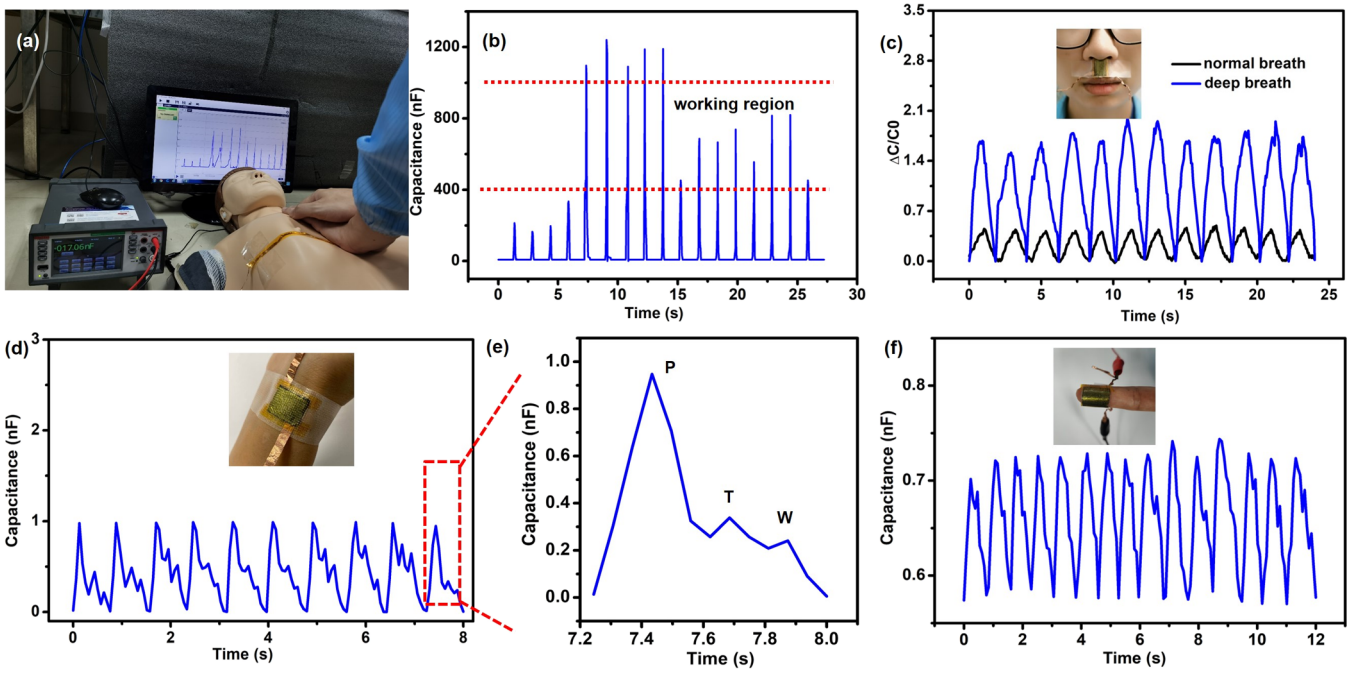

Figure 5. Employing the MDM iontronic pressure sensor for first-aid training. (a) Photograph of CPR testing on a training manikin. (b) Capacitance variation during the CPR process. (c) Relative capacitance change during the breath. (d) Capacitance signal of the wrist pulse in real-time and (e) zoom-in of one period from (d). (f) Capacitance signal of a finger pulse in real-time.

microstructures of random topography and size have more chance to interact with each other, further extending the support of external loading; (iii) with protrusive microstructures on both sides of each iontronic film, more layers help distribute the stress more uniformly across the entire dielectric film, as illustrated by the simulation result in Figure 3g. With these combined advantages, the MDM iontronic film design realized an ultrabroad linear sensing range.

The developed MDM iontronic capacitive pressure sensor with high sensitivity and the wide linear working range was applied for human body motion monitoring and vital signal detection. Figure 4 shows the detection of various body motions from low to high pressure. We attached the sensor to a volunteer's cheek to distinguish the facial expressions of smiling, laughing, and surprised, as shown in Figure 4a. Smiling and laughing shrink the zygomaticus differently, which leads to a small and large increase of the capacitance. However, when the volunteer expresses surprise, the zygomaticus releases that causes a decrease of the capacitance. Similarly, attaching the sensor to the face can also be used to recognize how people breathe. Inhaling by nose and mouth would lead to the release and shrink of the zygomaticus, resulting in a reverse capacitance change, as shown in Figure 4b,c. Besides facial motion, limb movements can be monitored as well. For instance, bending the arms upward will lead to tension in the biceps. Thus, fixing the fabricated flexible pressure sensor on such muscle would distinguish the different bending angles of the arm. Figure 4d presents the repeated bending-flatting of the arm with an upward bending of approximately 45 and 90°, respectively. The sensor exhibits a stable performance under dynamic movements and can separate the bending angles of the arms. The ultrawide working range of the sensor allows it to be used for walking detection. The sensor is pasted on the volunteer's foot (inset of Figure 4e) to detect the tiptoe and stepping of the heel. During walking, part of the body weight will be exerted to the sensor, and the periodic capacitance variation in Figure 4e indicates the lift-off and landing of the foot, proving the real capability of walking monitoring and step counting.

Taking the advantage of the high sensitivity and ultrabroad linear working range, we also applied the sensor is in the CPR training procedure, in which pressure monitoring from extremely low to extremely high levels is required. As an emergency lifesaving medical treatment, CPR activates cardiac arrest using chest compression. The compression depth of the chest to implement a proper CPR should be 5−6 cm for an adult. Therefore, real-time pressure monitoring of the chest compression procedure is crucial to ensure the depth is within the proper range. The MDM iontronic pressure sensor is attached to the center of an adult CPR training manikin chest. Subsequently, two hands with the fingers crossed are pushed hard and fast to the position where the pressure sensor is located as demonstrated in Figure 5a. According to a reported study,[54] the compression force is about 400−1000 N (335−1090 kPa), which corresponds to a 400 to 1000 nF capacitance change for our sensor. Figure 5b shows the pressure monitoring of the CPR procedure. Initially, the compression pressure was smaller than the minimal required level, thus, the volunteer pushed harder to increase the force. Noticed from the sensor response that the compression pressure exceeded the maximum required level, which may cause damage to the victims, the volunteer slightly decreased the pushing force correspondingly, and as reflected by the pressure sensor that the force located in the proper region.

To evaluate the implementation of CPR, vital signs such as the breath rate, wrist pulse, and blood pressure of the victims should be monitored after 2 min of chest compressions. Owing to the high sensitivity of the MDM iontronic pressure sensor, it can be used to detect a series of physiological signals. First, the sensor is attached to the middle between the upper lip and

https://doi.org/10.1021/acssensors.0c02547
ACS Sens. 2021, 6, 1785−1795

nose for breath detection. When the volunteer breathes, the capacitance of the sensor varies periodically as a result of airflow pressure. Figure 5c shows the relative capacitance change during the breath that normal and deep breath can be distinguished by capacitance variation. Moreover, the breath rate is calculated to be 18 per minute, which is in the range of a healthy adult.

The wrist pulse is an important indicator of cardiac beating, which can also be monitored by the sensor. Attaching the sensor to the wrist of a volunteer, the pulse signal was recorded as shown in Figure 5d. The percussion wave (P-wave), tidal wave (T-wave), valley, and diastolic wave (D-wave) are related to the systolic/diastolic blood pressure demonstrated in Figure 5e. The heart rate of the volunteer can be calculated as 75 beats/min. The heart rate can also be monitored from the finger. Taking advantage of high flexibility, the sensor is enwound on the volunteers' index finger as shown in Figure 5f. The heart rate detected from finger is also 75 beats/min, which is consistent with the pulse signal. The above results imply our sensor can be integrated into first-aid systems to monitor a variety of vital signs, from extremely low-pressure loading to sufficiently high-pressure loading conditions. The sensor can also be used to monitor extremely high-pressure scenarios such as the tactile operations of a heavy industrial robot and the dynamic pressure of a fast speed sport.

CONCLUSIONS

In summary, we developed a flexible iontronic pressure sensor with MDM ionic gel films. The stacking of films with protrusive microstructures on both sides formed gaps of random topography and size between the adjacent films, which distribute the applied load uniformly and support the pressure to a large extent, resulting in a linear working range from 0.013 to 2063 kPa. In addition, the EDL with densely distributed protrusive microstructures at the interface contributes to a high sensitivity (9.17 kPa^{-1}) and a fast response time (5 ms) within the entire linear working range. To the best of our knowledge, this is the first demonstration of a highly sensitive and fast responding flexible sensor that can measure pressure loading across 6 orders of magnitude. The sensor also showed high stability with no degradation over 5,000 loading/unloading cycles. The ultrabroad linear working range enables accurate and stable sensing in both low-pressure and high-pressure scenarios, without the need for recalibration. As such, the proposed sensor can be used in diverse applications including wearable devices, electronic skin of robots, and human−machine interfaces.

ASSOCIATED CONTENT

Supporting Information

The Supporting Information is available free of charge at https://pubs.acs.org/doi/10.1021/acssensors.0c02547.

Ion gel design and the fabrication process of the MDM iontronic sensor; maximum sensitivity of the sensor as a function of iontronic film layer number; relative capacitance changes as a function of pressure applied to the MDM iontronic sensor prepared using grit #400 and 12 layers of iontronic film as the dielectric layer; lower working limit, frequency response, and hysteresis test of sensor; initial capacitance of sensor after each cyclic loading/unloading test; and detailed parameter values of eqs1 and 2 (PDF)

AUTHOR INFORMATION

Corresponding Authors

Zhengchun Peng − *Key Laboratory of Optoelectronic Devices and Systems of Ministry of Education and Guangdong Province, College of Physics and Optoelectronic Engineering, Shenzhen University, Shenzhen 518060, China;* orcid.org/0000-0002-7114-1797; Email: zcpeng@szu.edu.cn

Weiguan Zhang − *Guangdong Provincial Key Laboratory of Micro/Nano Optomechatronic Engineering, College of Mechatronics and Control Engineering, Shenzhen University, Shenzhen 518060, China*; Email: weigzhang@szu.edu.cn

Authors

Yan Xiao − *Key Laboratory of Optoelectronic Devices and Systems of Ministry of Education and Guangdong Province, College of Physics and Optoelectronic Engineering, Shenzhen University, Shenzhen 518060, China*

Yu Duan − *Key Laboratory of Optoelectronic Devices and Systems of Ministry of Education and Guangdong Province, College of Physics and Optoelectronic Engineering, Shenzhen University, Shenzhen 518060, China*

Ning Li − *Key Laboratory of Optoelectronic Devices and Systems of Ministry of Education and Guangdong Province, College of Physics and Optoelectronic Engineering, Shenzhen University, Shenzhen 518060, China*

Linlin Wu − *Key Laboratory of Optoelectronic Devices and Systems of Ministry of Education and Guangdong Province, College of Physics and Optoelectronic Engineering, Shenzhen University, Shenzhen 518060, China*

Bo Meng − *Key Laboratory of Optoelectronic Devices and Systems of Ministry of Education and Guangdong Province, College of Physics and Optoelectronic Engineering, Shenzhen University, Shenzhen 518060, China*

Feihu Tan − *Key Laboratory of Optoelectronic Devices and Systems of Ministry of Education and Guangdong Province, College of Physics and Optoelectronic Engineering, Shenzhen University, Shenzhen 518060, China*

Yan Lou − *Guangdong Provincial Key Laboratory of Micro/Nano Optomechatronic Engineering, College of Mechatronics and Control Engineering, Shenzhen University, Shenzhen 518060, China;* orcid.org/0000-0001-8523-2932

Hao Wang − *Guangdong Provincial Key Laboratory of Micro/Nano Optomechatronic Engineering, College of Mechatronics and Control Engineering, Shenzhen University, Shenzhen 518060, China;* orcid.org/0000-0001-8896-5496

Complete contact information is available at: https://pubs.acs.org/10.1021/acssensors.0c02547

Author Contributions

Y.X. conceived the original idea, fabricated and characterized the device, and wrote the manuscript. Y.D., N.L., L.L.W.B.M., and F.H.T. assisted with the evaluation and application of the device. Z.C.P. and W.G.Z. provided regular guidance and key insight to the research including maturing the concept and the working mechanism, and revised the manuscript. All authors discussed the results and commented on the manuscript.

Notes

The authors declare no competing financial interest.

■ ACKNOWLEDGMENTS

This work was financially supported by the Science and Technology Innovation Commission of Shenzhen (JCYJ20190808142609414, KQTD20170810105439418, JCYJ20190808150401651, and JCYJ20170818091233245) the National Natural Science Foundation of China (61904112, 51675347, and 61671308), the Postdoctoral Science Foundation of China (2019M650209), and the Department of Education of Guangdong Province (2016KZDXM005).

■ REFERENCES

(1) Chortos, A.; Liu, J.; Bao, Z. Pursuing prosthetic electronic skin. *Nature Mater* **2016**, *15*, 937−950.
(2) Chen, Z.; Wang, Z.; Li, X.; Lin, Y.; Luo, N.; Long, M.; Zhao, N.; Xu, J.-B. Flexible piezoelectric-induced pressure sensors for static measurements based on nanowires/graphene heterostructures. *ACS Nano* **2017**, *11*, 4507−4513.
(3) Li, X.; Yang, T.; Yang, Y.; Zhu, J.; Li, L.; Alam, F. E.; Li, X.; Wang, K.; Cheng, H.; Lin, C.-T.; Fang, Y.; Zhu, H. Large-Area Ultrathin Graphene Films by Single-Step Marangoni Self-Assembly for Highly Sensitive Strain Sensing Application. *Adv. Funct. Mater.* **2016**, *26*, 1322−1329.
(4) Someya, T.; Sekitani, T.; Iba, S.; Kato, Y.; Kawaguchi, H.; Sakurai, T. A large-area, flexible pressure sensor matrix with organic field-effect transistors for artificial skin applications. *Proceedings of the National Academy of Sciences* **2004**, *101*, 9966−9970.
(5) Takei, K.; Takahashi, T.; Ho, J. C.; Ko, H.; Gillies, A. G.; Leu, P. W.; Fearing, R. S.; Javey, A. Nanowire active-matrix circuitry for low-voltage macroscale artificial skin. *Nature Mater* **2010**, *9*, 821−826.
(6) Hammock, M. L.; Chortos, A.; Tee, B. C.-K.; Tok, J. B.-H.; Bao, Z. 25th Anniversary Article: The Evolution of Electronic Skin (E-Skin): A Brief History, Design Considerations, and Recent Progress. *Adv. Mater.* **2013**, *25*, 5997−6038.
(7) Wang, X.; Dong, L.; Zhang, H.; Yu, R.; Pan, C.; Wang, Z. L. Recent progress in electronic skin. *Adv. Sci.* **2015**, *2*, 1500169.
(8) Boland, C. S.; Khan, U.; Backes, C.; O'Neill, A.; Mccauley, J.; Duane, S.; Shanker, R.; Liu, Y.; Jurewicz, I.; Dalton, A. B.; Coleman, J. N. Sensitive, High-Strain, High-Rate Bodily Motion Sensors Based on Graphene-Rubber Composites. *ACS Nano* **2014**, *8*, 8819−8830.
(9) Yang, W.; Chen, J.; Wen, X.; Jing, Q.; Yang, J.; Su, Y.; Zhu, G.; Wu, W.; Wang, Z. L. Triboelectrification based motion sensor for human-machine interfacing. *ACS Appl. Mater. Interfaces* **2014**, *6*, 7479−7484.
(10) Jung, S.; Kim, J. H.; Kim, J.; Choi, S.; Lee, J.; Park, I.; Hyeon, T.; Kim, D.-H. Reverse-Micelle-Induced Porous Pressure-Sensitive Rubber for Wearable Human-Machine Interfaces. *Adv. Mater.* **2014**, *26*, 4825−4830.
(11) Zang, Y.; Zhang, F.; Di, C.-a.; Zhu, D. Advances of flexible pressure sensors toward artificial intelligence and health care applications. *Mater. Horiz.* **2015**, *2*, 140−156.
(12) Wang, X.; Que, M.; Chen, M.; Han, X.; Li, X.; Pan, C.; Wang, Z. L. Full Dynamic-Range Pressure Sensor Matrix Based on Optical and Electrical Dual-Mode Sensing. *Adv. Mater.* **2017**, *29*, 1605817.
(13) Kim, S.; Amjadi, M.; Lee, T.-I.; Jeong, Y.; Kwon, D.; Kim, M. S.; Kim, K.; Kim, T.-S.; Oh, Y. S.; Park, I. Wearable, Ultrawide-Range, and Bending-Insensitive Pressure Sensor Based on Carbon Nanotube Network-Coated Porous Elastomer Sponges for Human Interface and Healthcare Devices. *ACS Appl. Mater. Interfaces* **2019**, *11*, 23639−23648.
(14) Mannsfeld, S. C. B.; Tee, B. C.-K.; Stoltenberg, R. M.; Chen, C. V. H.-H.; Barman, S.; Muir, B. V. O.; Sokolov, A. N.; Reese, C.; Bao, Z. Highly sensitive flexible pressure sensors with microstructured rubber dielectric layers. *Nature Mater* **2010**, *9*, 859−864.
(15) Bae, G. Y.; Pak, S. W.; Kim, D.; Lee, G.; Kim, D. H.; Chung, Y.; Cho, K. Linearly and Highly Pressure-Sensitive Electronic Skin Based on a Bioinspired Hierarchical Structural Array. *Adv. Mater.* **2016**, *28*, 5300−5306.
(16) Wei, Y.; Chen, S.; Lin, Y.; Yang, Z.; Liu, L. Cu-Ag core-shell nanowires for electronic skin with a petal molded microstructure. *J. Mater. Chem. C* **2015**, *3*, 9594−9602.
(17) Liu, M.; Pu, X.; Jiang, C.; Liu, T.; Huang, X.; Chen, L.; Du, C.; Sun, J.; Hu, W.; Wang, Z. L. Large-Area All-Textile Pressure Sensors for Monitoring Human Motion and Physiological Signals. *Adv. Mater.* **2017**, *29*, 1703700.
(18) Gong, S.; Schwalb, W.; Wang, Y.; Chen, Y.; Tang, Y.; Si, J.; Shirinzadeh, B.; Cheng, W. A wearable and highly sensitive pressure sensor with ultrathin gold nanowires. *Nat. Commun.* **2014**, *5*, 3132.
(19) Shi, J.; Wang, L.; Dai, Z.; Zhao, L.; Du, M.; Li, H.; Fang, Y. Multiscale hierarchical design of a flexible piezoresistive pressure sensor with high sensitivity and wide linearity range. *Small* **2018**, *14*, 1800819.
(20) Xiong, Y.; Shen, Y.; Tian, L.; Hu, Y.; Zhu, P.; Sun, R.; Wong, C.-P. A flexible, ultra-highly sensitive and stable capacitive pressure sensor with convex microarrays for motion and health monitoring. *Nano Energy* **2020**, *70*, 104436.
(21) Sharma, S.; Chhetry, A.; Sharifuzzaman, M.; Yoon, H.; Park, J. Y. Wearable Capacitive Pressure Sensor Based on MXene Composite Nanofibrous Scaffolds for Reliable Human Physiological Signal Acquisition. *ACS Appl. Mater. Interfaces* **2020**, *12*, 22212−22224.
(22) Yang, J.; Luo, S.; Zhou, X.; Li, J.; Fu, J.; Yang, W.; Wei, D. Flexible, tunable, and ultrasensitive capacitive pressure sensor with microconformal graphene electrodes. *ACS Appl. Mater. Interfaces* **2019**, *11*, 14997−15006.
(23) Park, K.-I.; Son, J. H.; Hwang, G.-T.; Jeong, C. K.; Ryu, J.; Koo, M.; Choi, I.; Lee, S. H.; Byun, M.; Wang, Z. L.; Lee, K. J. Highly-Efficient, Flexible Piezoelectric PZT Thin Film Nanogenerator on Plastic Substrates. *Adv. Mater.* **2014**, *26*, 2514−2520.
(24) Shin, K.-Y.; Lee, J. S.; Jang, J. Highly sensitive, wearable and wireless pressure sensor using free-standing ZnO nanoneedle/PVDF hybrid thin film for heart rate monitoring. *Nano Energy* **2016**, *22*, 95−104.
(25) Xu, S.; Qin, Y.; Xu, C.; Wei, Y.; Yang, R.; Wang, Z. L. Self-powered nanowire devices. *Nature Nanotech* **2010**, *5*, 366−373.
(26) Wu, W.; Wen, X.; Wang, Z. L. Taxel-addressable matrix of vertical-nanowire piezotronic transistors for active and adaptive tactile imaging. *Science* **2013**, *340*, 952−957.
(27) Lin, L.; Xie, Y.; Wang, S.; Wu, W.; Niu, S.; Wen, X.; Wang, Z. L. Triboelectric active sensor array for self-powered static and dynamic pressure detection and tactile imaging. *ACS Nano* **2013**, *7*, 8266−8274.
(28) Wang, X.; Liu, Z.; Zhang, T. Flexible sensing electronics for wearable/attachable health monitoring. *Small* **2017**, *13*, 1602790.
(29) Xu, F.; Li, X.; Shi, Y.; Li, L.; Wang, W.; He, L.; Liu, R. Recent developments for flexible pressure sensors: a review. *Micromachines* **2018**, *9*, 580.
(30) Li, J.; Bao, R.; Tao, J.; Peng, Y.; Pan, C. Recent progress in flexible pressure sensor arrays: from design to applications. *J. Mater. Chem. C* **2018**, *6*, 11878−11892.
(31) Keplinger, C.; Sun, J.-Y.; Foo, C. C.; Rothemund, P.; Whitesides, G. M.; Suo, Z. Stretchable, transparent, ionic conductors. *Science* **2013**, *341*, 984−987.
(32) Sun, J.-Y.; Keplinger, C.; Whitesides, G. M.; Suo, Z. Ionic skin. *Adv. Mater.* **2014**, *26*, 7608−7614.
(33) Cho, S. H.; Lee, S. W.; Yu, S.; Kim, H.; Chang, S.; Kang, D.; Hwang, I.; Kang, H. S.; Jeong, B.; Kim, E. H.; Cho, S. M.; Kim, K. L.; Lee, H.; Shim, W.; Park, C. Micropatterned pyramidal ionic gels for sensing broad-range pressures with high sensitivity. *ACS Appl. Mater. Interfaces* **2017**, *9*, 10128−10135.
(34) Qiu, Z.; Wan, Y.; Zhou, W.; Yang, J.; Yang, J.; Huang, J.; Zhang, J.; Liu, Q.; Huang, S.; Bai, N.; Wu, Z.; Hong, W.; Wang, H.; Guo, C. F. Ionic Skin with Biomimetic Dielectric Layer Templated from Calathea Zebrine Leaf. *Adv. Funct. Mater.* **2018**, *28*, 1802343.
(35) Chhetry, A.; Kim, J.; Yoon, H.; Park, J. Y. Ultrasensitive interfacial capacitive pressure sensor based on a randomly distributed

https://doi.org/10.1021/acssensors.0c02547
ACS Sens. 2021, 6, 1785−1795

microstructured iontronic film for wearable applications. *ACS Appl. Mater. Interfaces* **2019**, *11*, 3438−3449.
(36) Bai, N.; Wang, L.; Wang, Q.; Deng, J.; Wang, Y.; Lu, P.; Huang, J.; Li, G.; Zhang, Y.; Yang, J.; Xie, K.; Zhao, X.; Guo, C. Graded intrafillable architecture-based iontronic pressure sensor with ultra-broad-range high sensitivity. *Nat. Commun.* **2020**, *11*, 209.
(37) Li, S.; Chu, J. R.; Li, B.; Chang, Y.; Pan, T. Handwriting Iontronic Pressure Sensing Origami. *ACS Appl. Mater. Interfaces* **2019**, *11*, 46157−46164.
(38) Lee, Y.; Park, J.; Cho, S.; Shin, Y.-E.; Lee, H.; Kim, J.; Myoung, J.; Cho, S.; Kang, S.; Baig, C.; Ko, H. Flexible ferroelectric sensors with ultrahigh pressure sensitivity and linear response over exceptionally broad pressure range. *ACS Nano* **2018**, *12*, 4045−4054.
(39) Pyo, S.; Lee, J.; Kim, W.; Jo, E.; Kim, J. Multi-Layered, Hierarchical Fabric-Based Tactile Sensors with High Sensitivity and Linearity in Ultrawide Pressure Range. *Adv. Funct. Mater.* **2019**, *29*, 1902484.
(40) Oh, J.; Kim, J. O.; Kim, Y.; Choi, H. B.; Yang, J. C.; Lee, S.; Pyatykh, M.; Kim, J.; Sim, J. Y.; Park, S. Highly Uniform and Low Hysteresis Piezoresistive Pressure Sensors Based on Chemical Grafting of Polypyrrole on Elastomer Template with Uniform Pore Size. *Small* **2019**, *15*, 1901744.
(41) Shintake, J.; Piskarev, E.; Jeong, S. H.; Floreano, D. Ultrastretchable Strain Sensors Using Carbon Black-Filled Elastomer Composites and Comparison of Capacitive Versus Resistive Sensors. *Adv. Mater. Technol.* **2018**, *3*, 1700284.
(42) Chen, S.; Zhuo, B.; Guo, X. Large area one-step facile processing of microstructured elastomeric dielectric film for high sensitivity and durable sensing over wide pressure range. *ACS Appl. Mater. Interfaces* **2016**, *8*, 20364−20370.
(43) Pruvost, M.; Smit, W. J.; Monteux, C.; Poulin, P.; Colin, A. Polymeric foams for flexible and highly sensitive low-pressure capacitive sensors. *npj Flexible Electron.* **2019**, *3*, 7.
(44) Boutry, C. M.; Nguyen, A.; Lawal, Q. O.; Chortos, A.; Rondeau-Gagné, S.; Bao, Z. Pressure Sensors: A Sensitive and Biodegradable Pressure Sensor Array for Cardiovascular Monitoring (Adv. Mater. 43/2015). *Adv. Mater.* **2015**, *27*, 6953.
(45) Li, G.; Qiu, Z.; Wang, Y.; Hong, Y.; Wan, Y.; Zhang, J.; Yang, J.; Wu, Z.; Hong, W.; Guo, C. F. PEDOT:PSS/Grafted-PDMS Electrodes for Fully Organic and Intrinsically Stretchable Skin-like Electronics. *ACS Appl. Mater. Interfaces* **2019**, *11*, 10373−10379.
(46) Li, T.; Luo, H.; Qin, L.; Wang, X.; Xiong, Z.; Ding, H.; Gu, Y.; Liu, Z.; Zhang, T. Flexible capacitive tactile sensor based on micropatterned dielectric layer. *Small* **2016**, *12*, 5042−5048.
(47) Liu, W.; Yan, C. Direct printing of stretchable elastomers for highly sensitive capillary pressure sensors. *Sensors* **2018**, *18*, 1001.
(48) Yang, J.; Liu, Q.; Deng, Z.; Gong, M.; Lei, F.; Zhang, J.; Zhang, X.; Wang, Q.; Liu, Y.; Wu, Z.; Guo, C.F. Ionic liquid-activated wearable electronics. *Mater. Today Phys.* **2019**, *8*, 78−85.
(49) Tang, Z.; Scriven, L. E.; Davis, H. T. A three-component model of the electrical double layer. *The Journal of Chemical Physics* **1992**, *97*, 494−503.
(50) Zhang, S.; Lee, K. H.; Frisbie, C. D.; Lodge, T. P. Ionic conductivity, capacitance, and viscoelastic properties of block copolymer-based ion gels. *Macromolecules* **2011**, *44*, 940−949.
(51) Oldham, K. B. A Gouy-Chapman-Stern model of the double layer at a (metal)/(ionic liquid) interface. *Journal of Electroanalytical Chemistry* **2008**, *613*, 131−138.
(52) Nie, B.; Li, R.; Cao, J.; Brandt, J. D.; Pan, T. Flexible transparent iontronic film for interfacial capacitive pressure sensing. *Adv. Mater.* **2015**, *27*, 6055−6062.
(53) He, B.; Zhang, C.; Zhou, Y.; Wang, Z. A computing method to determine the performance of an ionic liquid gel soft actuator. *Applied Bionics and Biomechanics* **2018**, *2018*, 1.
(54) Hyun, S.-H.; Ryew, C.-C. Does maintain consistency with a high quality of cardiac compression force between diastole and systole phase? *J. Exerc. Rehabil.* **2019**, *15*, 334−338.

https://doi.org/10.1021/acssensors.0c02547
ACS Sens. 2021, 6, 1785−1795